



UNIVERSITY OF LEEDS

This is a repository copy of *Drained cavity expansion analysis with a unified state parameter model for clay and sand*.

White Rose Research Online URL for this paper:
<http://eprints.whiterose.ac.uk/126776/>

Version: Accepted Version

Article:

Mo, P-Q and Yu, H-S (2018) Drained cavity expansion analysis with a unified state parameter model for clay and sand. *Canadian Geotechnical Journal*, 55 (7). pp. 1029-1040. ISSN 0008-3674

<https://doi.org/10.1139/cgj-2016-0695>

This article is protected by copyright. All rights reserved. This is an author produced version of a paper published in the *Canadian Geotechnical Journal*. Uploaded in accordance with the publisher's self-archiving policy.

Reuse

Items deposited in White Rose Research Online are protected by copyright, with all rights reserved unless indicated otherwise. They may be downloaded and/or printed for private study, or other acts as permitted by national copyright laws. The publisher or other rights holders may allow further reproduction and re-use of the full text version. This is indicated by the licence information on the White Rose Research Online record for the item.

Takedown

If you consider content in White Rose Research Online to be in breach of UK law, please notify us by emailing eprints@whiterose.ac.uk including the URL of the record and the reason for the withdrawal request.



eprints@whiterose.ac.uk
<https://eprints.whiterose.ac.uk/>

1

2

3 **Drained cavity expansion analysis with a unified state**
4 **parameter model for clay and sand**

5

6 **Pin-Qiang Mo, Associate Research Scientist**

7 Email: pinqiang.mo@cumt.edu.cn

8 State Key Laboratory for GeoMechanics and Deep Underground Engineering

9 School of Mechanics and Civil Engineering, China University of Mining and Technology

10 No.1 Daxue Road, Xuzhou, Jiangsu, 221116, China

11

12 **Hai-Sui Yu, Professor of Geotechnical Engineering**

13 **and Pro-Vice-Chancellor**

14 Email: PVC.int@leeds.ac.uk

15 School of Civil Engineering, University of Leeds

16 Leeds, LS2 9JT, U.K.

17

18 submitted on 28 November 2017

19 approx. 4000 words

20 14 Figures and 4 Tables

21 **ABSTRACT**

22 This paper presents an analytical solution for drained expansion in both spherical and
23 cylindrical cavities with a unified state parameter model for clay and sand (CASM) (Yu, 1998).
24 The solution developed here provides the stress and strain fields during the expansion of a
25 cavity from an initial to an arbitrary final radius. Small strains are assumed to the elastic region
26 and large strains are applied for soil in the plastic region by using logarithmic strain definitions.
27 Since its development, the unified CASM model has been demonstrated by many researchers
28 to be able to capture the overall soil behaviour for both clay and sand under both drained and
29 undrained loading conditions. In this study, the CASM model is used to model soil behaviour
30 whilst we develop a drained cavity expansion solution with the aid of an auxiliary variable.
31 This is an extension of the undrained solution presented by the authors (Mo and Yu, 2017). The
32 parametric study investigates the effects of various model constants including the stress-state
33 coefficient and the spacing ratio on soil stress paths and cavity expansion curves. Both London
34 clay and Ticino sand are modelled under various initial stress conditions and initial state
35 parameters. The newly-developed analytical solution highlights the potential applications in
36 geotechnical practice (e.g. for the interpretation of cone penetration test (CPT) data) and also
37 serves as useful benchmarks for numerical simulations of cavity expansion problems in critical
38 state soils.

39

40 **KEYWORDS**

41 Cavity expansion analysis, analytical solution, drained analysis, unified state parameter model,
42 cone penetration test

43

44 List of notations provided on Page 3

45

46 NOTATION

a	radius of cavity
c	radius of the elastic/plastic boundary
e	void ratio of granular material
m	parameter to combine cylindrical ($m = 1$) and spherical ($m = 2$) analysis
n	stress-state coefficient for CASM
p', q	mean stress and deviatoric stress
p'_0	initial mean effective stress
p'_{y0}	preconsolidation pressure
r	radial position of soil element around the cavity
r^*	spacing ratio for the concept of state parameter
G	elastic shear modulus
K	elastic bulk modulus
R_0	isotropic overconsolidation ratio, defined as p'_{y0}/p'_0
χ	auxiliary independent variable, defined as u/r
δ, γ	volumetric and shear strains
$\varepsilon_p, \varepsilon_q$	volumetric and shear strains
$\varepsilon_r, \varepsilon_\theta$	radial and tangential strains
η	stress ratio, defined as q/p'
μ	Poisson's ratio of soil
v	specific volume, defined as $1 + e$
$\sigma'_r, \sigma'_\theta$	radial and tangential stresses
ξ	state parameter
ξ_R	reference state parameter
$M, \kappa, \lambda, \Gamma, \Lambda$	critical state soil parameters

48 INTRODUCTION

49 The cavity expansion method and its applications to geotechnical problems have been
50 extensively developed in the last five decades (e.g., Yu 2000). While early research ~~works~~ was
51 mainly focused on the expansion in elastic materials, analytical solutions have been developed
52 using increasingly more sophisticated constitutive soil models (e.g., Palmer and Mitchell 1971;
53 Vesic 1972; Carter et al. 1986; Yu and Houlsby 1991; Collins and Yu 1996; Chen and
54 Abousleiman 2012, 2013, 2016, 2017; Mo et al. 2014; Vrakas and Anagnostou 2014; Mo and
55 Yu 2017). As a result, the solutions have been particularly of interest to geotechnical
56 engineering problems, such as in-situ soil testing, pile foundations, and tunnelling, largely due
57 to their successful applications in providing simple but useful geotechnical solutions.

58 Perfect plasticity was initially adopted for cavity expansion in soils under either undrained or
59 drained conditions. Total stress analysis of cohesive soil is typically used for the Tresca and
60 von Mises materials, whereas the drained behaviour of soil is modelled by the effective stress
61 analysis for the Mohr Coulomb material. Among the solutions in elastic-perfectly plastic soils,
62 one of the milestones in cavity expansion solutions was provided by Yu and Houlsby (1991),
63 who derived a unified analytical solution of cavity expansion in dilatant elastic-plastic soils,
64 using the Mohr-Coulomb yield criterion with a non-associated flow rule. The large strain
65 analysis in the plastic region, with the aid of a series expansion, was used to derive a rigorous
66 closed-form solution for both cylindrical and spherical cavities. However, to account for the
67 variation of soil strength during cavity expansion, a solution using a strain-hardening/softening
68 plasticity model was clearly necessary.

69 As the most widely used strain-hardening or softening models in soil mechanics, critical state
70 soil models (Schofield and Wroth 1968) have been used to derive cavity expansion solutions
71 under both drained and undrained conditions in the last two decades (e.g., Collins and Yu 1996;
72 Cao et al. 2001; Chen and Abousleiman 2012, 2013, 2016; Mo and Yu 2017). It should be noted
73 that drained cavity expansion solutions in critical state soils are very limited due to the unknown
74 stress paths and variations of the specific volume during the cavity expansion process. Palmer
75 and Mitchell (1971) were the first to derive an approximate small-strain analytical solution for
76 cylindrical cavity expansion in normally consolidated clay. Similarity solutions for drained
77 cavities from zero initial radius in critical state soils were presented by Collins et al. (1992) and
78 Collins and Stimpson (1994), who provided the limit cavity pressures for both spherical and
79 cylindrical cavities. However, the asymptotic solutions are only valid for large cavity expansion
80 due to the approach of geometric self-similarity. Other similarity solutions were also developed
81 by Russell and Khalili (2002) using the conventional Mohr-Coulomb failure criterion and a
82 state parameter sand behaviour model with a non-linear critical state line. More recently, semi-

83 analytical solutions for crushable granular materials were proposed by Jiang and Sun (2012)
84 using a new critical state line, with a state-dependent dilatancy and a bounding surface
85 plasticity model. Again, similarity transformation was introduced for the cavity expansion
86 solutions, and plastic deformation was assumed as zero for constant stress ratio.

87 By abandoning the assumption of similarity, drained solutions for the expansion of cylindrical
88 cavities in the Modified Cam-clay and bounding surface plasticity soils were reported by Chen
89 and Abousleiman (2013, 2016), with the aid of an auxiliary variable in the plastic region, which
90 aims to convert the Eulerian formulation into Lagrangian form. The approach of auxiliary
91 variable is also applied to the proposed drained solutions for the general shear strain
92 hardening/softening Drucker-Prager models (Chen and Abousleiman, 2017) and for the unified
93 hardening parameter-based critical state model (Li et al. 2017). However, as pointed out by Yu
94 (1998) among others, it is also true that the conventional critical state models are less suitable
95 for modelling sand behaviour and heavily overconsolidated clays. Hence existing solutions for
96 cavity expansion for a unified critical state soil model for clay and sand are still limited.

97 In the present paper, an analytical solution for the expansion of both spherical and cylindrical
98 cavities with a unified state parameter model for clay and sand (CASM) (Yu, 1998) is
99 developed. This is an extension of the undrained cavity expansion solutions of Mo and Yu
100 (2017) to drained loading conditions. After introducing the unified state parameter model
101 CASM, the small strain theory is applied in the elastic region, and the large strain assumption
102 is used for soil in the plastic region. The approach of auxiliary variable used by Chen and
103 Abousleiman (2013) is employed for our drained analysis, which is valid for the expansion of
104 either a spherical or a cylindrical cavity in clay or sand material. In this paper, the results of
105 cavity expansion in both London clay and Ticino sand are presented for stress paths and cavity
106 expansion curves. A parametric study is also provided to investigate the effects of the stress-
107 state coefficient and the spacing ratio, as well as the effects of initial stress condition and initial
108 state parameter of the soil. The interpretation of CPT data using the proposed solution is also
109 compared with data from relevant calibration chamber tests.

110

111 PROBLEM DESCRIPTION

112 A spherical or cylindrical cavity with initial radius a_0 in an infinite soil (Fig. 1a) is assumed to
113 be expanded under fully drained conditions. As reported in Mo and Yu (2017), Fig. 1b
114 schematically illustrates the geometry and kinematics of cavity expansion. The initial stress
115 state is assumed as isotropic, with $\sigma'_{r,0} = \sigma'_{\theta,0} = p'_0$. For the cylindrical case, $\sigma'_{z,0}$ is equal to p'_0 ,
116 and the effect of σ'_z is not included in this study. For soil with an overconsolidated stress history,

117 the preconsolidation pressure is referred to as p'_{y0} , and $R_0 = p'_{y0}/p'_0$ represents the isotropic
 118 overconsolidation ratio in terms of the mean effective stress. The initial specific volume is
 119 referred to as v_0 , and the specific volume varies during the process of expansion for the drained
 120 analysis. Note that a compression positive notation is used throughout this paper, consistent
 121 with the undrained solution of Mo and Yu (2017).

122 For cavity expansion problems, the stresses of soil must satisfy the following quasi-static
 123 equilibrium equation:

$$124 \quad \sigma'_\theta - \sigma'_r = \frac{r}{m} \frac{d \sigma'_r}{d r} \quad (1)$$

125 where the parameter ‘ m ’ is used to integrate both spherical ($m = 2$) and cylindrical ($m = 1$)
 126 scenarios (following Yu and Houlsby 1991, Collins and Yu 1996, and Mo and Yu 2017); σ'_r
 127 and σ'_θ are the effective radial and tangential stresses, and r is the radius of the material element
 128 (r_0 is the initial position before cavity expansion). The symbol ‘ d ’ denotes the Eulerian
 129 derivative for every material particle at a specific moment.

130 According to Collins and Yu (1996), the mean and deviatoric effective stresses (p' ; q) for
 131 cavity expansion problems can be defined as follows:

$$132 \quad \begin{aligned} p' &= \frac{\sigma'_r + m \cdot \sigma'_\theta}{1+m} \\ q &= \sigma'_r - \sigma'_\theta \end{aligned} \quad (2)$$

133 Accordingly, the volumetric and shear strains (δ ; γ) can be written as:

$$134 \quad \begin{aligned} \delta &= \varepsilon_r + m \cdot \varepsilon_\theta \\ \gamma &= \varepsilon_r - \varepsilon_\theta \end{aligned} \quad (3)$$

135 As stated in Mo and Yu (2017), the definitions of ‘ p' ’, ‘ q ’ provided in eq. (2) and ‘ δ ’, ‘ γ ’ in
 136 eq. (3) are used consistent with the solution of Collins and Yu (1996), which can contribute to
 137 the simplification of the analytical solutions. For the problem with an isotropic in-situ stress
 138 state, the possible error introduced by this simplification has been shown to be negligible by a
 139 rigorous numerical (finite element) simulation (Sheng et al. 2000), which has also been reported
 140 by Chen and Abousleiman (2012).

141 Considering plastic soil behaviour, the strains are decomposed additively into elastic and plastic
 142 components. The superscripts ‘ e ’ and ‘ p ’ are used to distinguish the elastic and plastic
 143 components of the total strains. According to Collins and Stimpson (1994), the deformation in
 144 the elastic region is in fact isochoric with no volumetric change, although the material is
 145 compressible. Thus, the small strain analysis is used for soil in the elastic region, as expressed:

146
$$\begin{aligned}\varepsilon_r &= -\frac{du}{dr} \\ \varepsilon_\theta &= -\frac{u}{r}\end{aligned}\tag{4}$$

147 where u is the radial displacement. Conversely, to accommodate the effect of large deformation
148 in the cavity expansion process, the large strain analysis is adopted for the plastic regions by
149 assuming logarithmic strains (which are also termed true strains or Hencky strains):

150
$$\begin{aligned}\varepsilon_r &= -\ln\left(\frac{dr}{dr_0}\right) \\ \varepsilon_\theta &= -\ln\left(\frac{r}{r_0}\right)\end{aligned}\tag{5}$$

151

152 UNIFIED STATE PARAMETER MODEL

153 The unified state parameter model (CASM, developed by Yu 1998) is briefly described in this
154 section, which was also provided in Mo and Yu (2017). The critical state line is fully defined
155 as:

156
$$\begin{aligned}q &= M p' \\ v &= \Gamma - \lambda \ln p'\end{aligned}\tag{6}$$

157 where q and p' are the deviatoric and mean effective stresses; M is the slope of the critical state
158 line in $p' - q$ space; $v = 1 + e$ is the specific volume, and e is the void ratio; λ , κ and Γ are the
159 critical state constants.

160 The state parameter ξ is defined by Wroth and Bassett (1965) and Been and Jefferies (1985) as
161 the vertical distance between the current state and the critical state line in $\ln p' - v$ space (see
162 Fig. 2a):

163
$$\xi = v + \lambda \ln p' - \Gamma\tag{7}$$

164 With benefits of the concept of state parameter, Yu (1998) proposed a unified state parameter
165 model for clay and sand, which is referred to as CASM. The state boundary surface of the
166 CASM is described as:

167
$$\left(\frac{\eta}{M}\right)^n = 1 - \frac{\xi}{\xi_R}\tag{8}$$

168 where $\eta = q/p'$ is known as the stress ratio; n is the stress-state coefficient, which is a new
169 material constant and typically ranges between 1.0 ~ 5.0; $\xi_R = (\lambda - \kappa) \ln r^*$, is the reference
170 state parameter; and r^* is the spacing ratio, defined as p'_y/p'_x (Fig. 2a). Equation (8) also

171 represents the stress-state relation and the yield function. In terms of the preconsolidation
 172 pressure p'_y , the yield surface can be rewritten as follows:

$$173 \quad \left(\frac{\eta}{M}\right)^n = -\frac{\ln(p'/p'_y)}{\ln r^*} \quad (9)$$

174 The variation of state boundary surfaces (eq. (9)) with the stress-state coefficient are shown in
 175 Fig. 2b, with normalisation of the preconsolidation pressure. Rowe's stress-dilatancy relation
 176 (Rowe 1962), as expressed by:

$$177 \quad \frac{D \delta^p}{D \gamma^p} = \frac{9(M-\eta)}{9+3M-2M\eta} \times \frac{m}{m+1} \quad (10)$$

178 is adopted to define the plastic potential, which has been widely accepted with greatest success
 179 in describing the deformation of sands and other granular media. The symbol ' D ' denotes the
 180 Lagrangian derivative for a given material particle. The hardening law is then adopted based
 181 on a typical isotropic volumetric plastic strain hardening, as shown to be:

$$182 \quad D p'_y = \frac{\nu p'_y}{\lambda - \kappa} D \delta^p \quad (11)$$

183 It should be noted that the adopted soil model CASM after Yu (1998) could be taken as a basis
 184 for further extensions; e.g. to include shear hardening, to include viscoplasticity, for unsaturated
 185 soils, for bounded geomaterials, etc. (see Yu, 2006). In terms of a general three-dimensional
 186 stress state, M value varying with Lode's angle (proposed by Sheng et al., 2000) could also be
 187 included in the yield function, capturing more realistic soil behaviour under various loading
 188 paths. This paper, however, focuses on the derivation of drained cavity expansion with the
 189 original proposed soil model CASM, largely owing to the simple stress paths of spherical and
 190 cylindrical cavity expansion.

191

192 ANALYTICAL SOLUTION

193 The drained analytical solution is provided in this section, for a cavity expanded from a_0 to a .
 194 After a certain expansion, the soil medium around the cavity becomes plastic, and the plastic
 195 region develops from the cavity wall. The symbol ' c ' is the radius of the elastic-plastic
 196 boundary; thus, for $r > c$, soil is in the elastic region, and the plastic region is for soil at $a <$
 197 $r < c$ (see Fig. 1).

198 Solution for soil in the elastic region

199 To describe the stress-strain relationship in the elastic region, the elastic strain rates are
 200 expressed as follows:

$$\begin{aligned}
201 \quad D \delta^e &= \frac{1}{K} D p' \\
D \gamma^e &= \frac{1}{2G} D q
\end{aligned} \tag{12}$$

202 where K is the elastic bulk modulus, which is equal to $\nu p'/\kappa$; G is the elastic shear modulus
203 for an isotropic linear elastic material as defined by Collins and Stimpson (1994), which is
204 determined as:

$$205 \quad G = \frac{(1+m)(1-2\mu)\nu p'}{2[1+(m-1)\mu]\kappa} \tag{13}$$

206 Based on the assumption of small strains, the distributions of effective stresses in the elastic
207 region can be expressed as follows, according to the solution of Yu and Houlsby (1991):

$$\begin{aligned}
208 \quad \sigma'_r &= p'_0 + B_1 \times \frac{1}{r^{1+m}} \\
\sigma'_\theta &= p'_0 - B_1 \times \frac{1}{m r^{1+m}}
\end{aligned} \tag{14}$$

209 where B_1 is a constant of integration. And the distributions of strains in the elastic region can
210 be solved as:

$$\begin{aligned}
211 \quad \delta &= 0 \\
\gamma &= B_2 \times B_1 \times \frac{1+m}{\nu_0 p'_0 m r^{1+m}}
\end{aligned} \tag{15}$$

212 where $B_2 = [1 + (m - 1) \mu] \kappa / [(1 + m) (1 - 2 \mu)]$. For the elastic stage (i.e. there is no
213 plastic region), B_1 can be derived based on the boundary condition: $\varepsilon_\theta|_{r=a} = -(a - a_0)/a$,
214 which results in $B_1 = \nu_0 p'_0 m a^m (a - a_0) / B_2$. However, for the plastic stage, the elastic-
215 plastic boundary is located at $r = c$, and the initial yielding deviatoric stress can be found from
216 the initial yield surface: $q_c = (\ln R_0 / \ln r^*)^{1/n} M p'_0$. The boundary condition at $r = c$ gives
217 that $B_1 = q_c m c^{1+m} / (1 + m)$ for the plastic stage, and the size of the plastic region c needs
218 to be determined based on the solution for the plastic region.

219

220 Solution for soil in the plastic region

221 Note that for soil in the plastic region ($a < r < c$), the elastic moduli (K and G) are not
222 constants but functions of the mean effective stress p' . The volumetric strain is related to the
223 specific volume: $\delta = -\ln(\nu/\nu_0)$. In order to convert the Eulerian formulation (e.g. eq. (1)) to
224 the Lagrangian description, a suitable auxiliary independent variable, $\chi = u/r = (r - r_0)/r$,
225 is introduced according to Chen and Abousleiman (2013). For the exact solution in the plastic
226 region, numerical integration is required from the elastic-plastic boundary ($r = c$), where the
227 initial yielding conditions are known with $p' = p'_0$, $q = q_c$, $\nu = \nu_0$, and $\chi = (c - c_0)/c =$

228 $B_2 q_c / [(1 + m) v_0 p'_0]$. For a given derivative $D \chi$, three formulations need to be established
 229 to relate $D \chi$ with $D p'$, $D q$, and $D v$, which will be derived from the equilibrium equation, the
 230 volumetric strain rate, and the deviatoric strain rate, respectively.

231 Together with the assumption of large strains (eq. (5)), the expression of strains can be
 232 converted into the forms of χ , as follows:

$$\begin{aligned} \varepsilon_\theta &= -\ln\left(\frac{r}{r_0}\right) = \ln(1 - \chi) \\ \varepsilon_r &= \delta - m \varepsilon_\theta = -\ln\left(\frac{v}{v_0}\right) - m \ln(1 - \chi) = -\ln\left[\frac{v}{v_0}(1 - \chi)^m\right] \\ \gamma &= -\ln\left[\frac{v}{v_0}(1 - \chi)^{m+1}\right] \end{aligned} \quad (16)$$

234 • Equilibrium equation

235 By using the auxiliary independent variable, the equilibrium equation (eq. (1)) can thus be
 236 rewritten as:

$$-q = \frac{r}{m} \frac{D\left(p' + \frac{m}{m+1}q\right)}{D\chi} \frac{d\chi}{dr} \quad (17)$$

238 and

$$\frac{r}{d} \frac{d\chi}{dr} = -\frac{u}{r} + \frac{du}{dr} = -\chi + \frac{du}{dr} \quad (18)$$

240 where du/dr can be obtained from the expression of $\varepsilon_r = \ln(1 - du/dr)$ together with eq.
 241 (16), i.e. $du/dr = 1 - v_0/[v(1 - \chi)^m]$. Therefore, the formulation based on the equilibrium
 242 equation is derived as:

$$-q = \frac{D p' + \frac{m}{m+1} D q}{m D \chi} \left[1 - \chi - \frac{v_0}{v(1 - \chi)^m}\right] \quad (19)$$

244 • Volumetric strain rate

245 The volumetric strain rate in the plastic region indicates the rate of specific volume (i.e. $D \delta =$
 246 $-D v / v$), which is also a combination of elastic and plastic components:

$$D \delta = -D v / v = D \delta^e + D \delta^p = \kappa \times \frac{D p'}{v p'} + \frac{\lambda - \kappa}{v} \frac{D p'_y}{p'_y} \quad (20)$$

248 The integration together with the yield criterion (eq. (9)) is equivalent to the expression of the
 249 state parameter (eq. (7)), which gives:

$$v = v_0 - \lambda \ln \frac{p'}{p'_0} + (\lambda - \kappa) \left[\ln R_0 - \left(\frac{\eta}{M}\right)^n \ln r^* \right] = C_1 + C_2 \ln p' + C_3 \eta^n \quad (21)$$

251 where

$$\begin{aligned} C_1 &= v_0 + \lambda \ln p'_0 + (\lambda - \kappa) \ln R_0 \\ C_2 &= -\lambda \\ C_3 &= -(\lambda - \kappa) \ln r^* / M^n \end{aligned} \quad (22)$$

253 The derivative form can then be rewritten as:

$$254 \quad D v = C_2 \frac{1}{p'} D p' + C_3 n \eta^{n-1} \left(\frac{1}{p'} D q - \frac{q}{p'^2} D p' \right) \quad (23)$$

255 • Deviatoric strain rate

256 Similarly, the deviatoric strain rate is thus further expressed as:

$$257 \quad D \gamma = -\frac{D v}{v} + \frac{m+1}{1-\chi} D \chi = D \gamma^e + D \gamma^p = B_2 \frac{D q}{v p'} + \frac{\lambda-\kappa}{v} \frac{D p'_y}{p'_y} \frac{9+3 M-2 M \eta}{9(M-\eta)} \frac{m+1}{m} \quad (24)$$

258 Therefore, the three formulations (eqs. (19), (23), and (24)) provide the increments of $D p'$, $D q$,
259 and $D v$ for a given $D \chi$ from $\chi|_{r=c}$ to $\chi|_{r=a} = (a - a_0)/a$. Thus, the distributions of v , χ ,
260 stresses and strains in the plastic region are obtained from the numerical integration. The
261 equivalent location of a material particle around the cavity r corresponding to the auxiliary
262 variable χ is revived by integration from a to r :

$$263 \quad \int_a^r \frac{d r}{r} = \ln \frac{r}{a} = \int_{\chi|_{r=a}}^{\chi} \frac{d \chi}{1-\chi-v_0/[v(1-\chi)^m]} \quad (25)$$

264 The elastic/plastic boundary c is also obtained from eq. (25) by integration from a to c , which
265 is used to determine B_1 and the distributions in the elastic region (eqs. (14) and (15)).

266

267 RESULTS AND DISCUSSION

268 Validation of the analytical solution

269 After examining the state boundary surface and the stress-state relation, the Modified Cam-clay
270 model could be accurately recovered by choosing $r^* = 2.0$ and a suitable value of $n \approx 1.5 -$
271 2.0 , as noted by Yu (1998). The validation of the proposed solution is performed by the
272 comparisons of the cylindrical cavity expansion between the recovered Modified Cam-clay
273 analysis and the results of exact analytical solution for the Modified Cam-clay model, which
274 were reported by Chen and Abousleiman (2013) in conjunction with their drained analysis. The
275 test with an isotropic in-situ stress condition was adopted for $R_0 = 3$. The parameters were
276 selected to be equivalent to those in Chen and Abousleiman (2013), as summarised in Table 1.

277 The stress paths, the distributions of stresses and specific volume are presented in Fig. 3, with
 278 comparisons of data from Chen and Abousleiman (2013), which was also verified by the finite
 279 element simulation. Note that all stress paths presented in this paper are provided for the soil
 280 element at the cavity wall. As the solution is quasi-static and time-independent, all soil elements
 281 follow the same stress path, but at any stage of the cavity expansion those elements closer to
 282 the cavity boundary are further along that path. The present analytical solution is thus validated
 283 by the close agreement between the calculated behaviour of the cavity expansion and the
 284 verified analytical results, although the Modified Cam-clay model is assumed by matching the
 285 state boundary surface and the stress-state relation using the CASM and the differences on the
 286 flow rules.

287

288 Drained cavity expansion in clay

289 This section describes the results of drained cavity expansion in clay using the CASM, for both
 290 spherical and cylindrical scenarios. Unless stated otherwise, all results are presented by
 291 choosing the material constants similar to those of London clay, as suggested by Yu (1998).
 292 The soil model parameters and the initial conditions for London clay are listed in Table 2. Note
 293 that the frictional constant M is determined by the critical state friction angle, using $M =$
 294 $2(m+1)\sin\phi_{cs}/[(m+1)-(m-1)\sin\phi_{cs}]$; ϕ_{cs} is also assumed based on the triaxial
 295 critical state friction: $\phi_{cs} = \phi_{tx}$ for spherical scenario and $\phi_{cs} = 1.125\phi_{tx}$ for cylindrical
 296 scenario, as suggested by Wroth (1984).

297 Fig. 4 shows the stress paths in normalised $p' - q$ space for $a/a_0 = 1$ to 10 with the variation
 298 of overconsolidation ratio R_0 , keeping the initial specific volume constant as 2.0. The critical
 299 state lines and initial yield surfaces for the tests with different values of R_0 overlap in
 300 normalised $p' - q$ space, and all stress paths start from $q = 0$ and gradually approach the
 301 critical state line. The critical state is reached only when the conditions are satisfied: $q/p' =$
 302 $Dq/Dp' = M$. It can be seen that the normalised stresses (i.e. p'/p'_{y0} , $q/(M \cdot p'_{y0})$) increase
 303 with the overconsolidation ratio, and slightly higher normalised stresses are found for the
 304 spherical tests comparing to the cylindrical tests.

305 The cavity expansion curves for $a/a_0 = 1$ to 10 are presented in Fig. 5 for both spherical and
 306 cylindrical scenarios, respectively; while the variations of the elastic-plastic radius c with the
 307 overconsolidation ratio R_0 are shown in Fig. 6. It is clear that the normalised cavity pressure
 308 (σ'_r/p'_0) increases with the overconsolidation ratio, whereas the elastic-plastic radius appears to
 309 be smaller for the test with a higher overconsolidation ratio. The limiting cavity pressure and
 310 the constant ratio of c/a are obtained after expansion of approximately 4 times of the initial

311 cavity size, while the cylindrical tests seem to require larger expansion before reaching the
312 limiting values. In addition, comparing to the spherical scenario, the cylindrical tests have lower
313 normalised cavity pressure but larger elastic-plastic radius.

314 With benefits of the CASM which can be recovered to the Original Cam-clay ($n = 1$ and $r^* =$
315 2.7183), the effects of model constants n and r^* are investigated by comparing the modelled
316 London clay and the Original Cam-clay. The results of stress paths and cavity expansion curves
317 for both $R_0 = 1$ and 16 are shown in Figs. 7-8, respectively. The difference on the yield surfaces
318 results in the loci of stresses and cavity expansion curves for both London clay and the Original
319 Cam-clay. Higher normalised stresses and limiting cavity pressure are found for London clay
320 with $R_0 = 1$, whereas the tests of the Original Cam-clay show higher values of normalised
321 stresses and limiting cavity pressure for heavily overconsolidated clay. It is clear that the
322 analytical solution with the CASM can be used for materials with different softening/hardening
323 responses, by modifying the values of stress-state coefficient n and spacing ratio r^* .

324

325 Drained cavity expansion in sand

326 Similarly, the results of drained cavity expansion in sand using the CASM are described in this
327 section, which are presented by choosing the material constants similar to those of Ticino sand,
328 as suggested by Yu (1998). The soil model parameters for Ticino sand and the initial conditions
329 under $p'_0 = 200 \text{ kPa}$ are listed in Table 3.

330 To investigate the effect of initial state parameter, ξ_0 from -0.075 to 0.075 is examined under a
331 constant initial mean stress of 200 kPa . Note that $\xi_0 = 0.075$ indicates the initial condition at
332 the normal compression line, since the reference state parameter $\xi_R = 0.075$. The results of the
333 cavity expansion curves and stress paths in $\ln p' - v$ space are presented in Figs. 9-10,
334 respectively. It is shown that the increase of initial state parameter reduces the limiting cavity
335 pressure and increases the limiting specific volume on the critical state line. Comparing to the
336 spherical tests, the value of limiting cavity pressure for the cylindrical scenario is about half of
337 that of the spherical scenario, which also results in a higher specific volume in Fig. 10.

338 The effect of initial mean stress is also investigated by varying p'_0 from 200 kPa to 800 kPa for
339 ξ_0 of both -0.075 and 0.075 . The corresponding soil parameters and the initial conditions are
340 provided in Table 4, and the stress paths in $\ln p' - v$ space are illustrated in Fig. 11 for both
341 spherical and cylindrical scenarios, respectively. Clearly, apart from the initial state parameter,
342 the initial stress condition has a large influence on the stress-strain relationship for soil around
343 the cavity.

344 Furthermore, the effects of the model constants n and r^* are illustrated in Figs. 12-13, for the
 345 results of cavity expansion curves and stress paths in $\ln p' - v$ space, respectively. By varying
 346 the stress-state coefficient n between 2 and 4, and the spacing ratio r^* between 108.6 and 1000,
 347 different softening responses of sand can be satisfactorily modelled, as suggested by Yu (1998).
 348 Thus the responses of cavity expansion in Fig. 12 show that the increase of either n or r^* can
 349 reduce the limiting cavity pressure for $\xi_0 = -0.075$, while the limiting cavity pressure
 350 increases with n and r^* for $\xi_0 = 0.075$. The stress paths in Fig. 13 present different loci of
 351 $\ln p' - v$ relation, while the difference of loci for $\xi_0 = 0.075$ is significantly larger than that of
 352 $\xi_0 = -0.075$. Correspondingly, the limiting state of specific volume decreases with n and r^*
 353 for $\xi_0 = 0.075$, and the reverse trends are found for $\xi_0 = -0.075$.

354

355 Potential geotechnical applications

356 Note that the proposed solution provides a general approach for drained cavity
 357 expansion/contraction problems using the critical state soil models, with the concept of state
 358 parameter and two additional soil parameters. The current solution with an arbitrary cavity
 359 expansion has major potential applications, including cone penetration tests, pressuremeter tests,
 360 pile foundations, tunnelling, and wellbore instability. Moreover, the solution serves as a
 361 benchmark for validating numerical simulations of boundary value problems.

362 A simple example for application to the interpretation of CPT data has been provided here using
 363 the developed analytical solution. The cone penetration testing in the calibration chambers is
 364 widely accepted as a versatile tool for interpretation between penetration resistance and soil
 365 properties. The cone tip resistance q_c is one of the main test measurements, which is usually
 366 related to the in situ effective stress and soil density. The approach of spherical cavity expansion
 367 idealises the cone penetration as an analogy of the expanded cavity under the same conditions
 368 by Vesic (1977) and Yu and Mitchell (1998) amongst many others. The cone resistance can
 369 therefore be predicted based on the calculated cavity pressure (Ladanyi and Johnson, 1974):

$$370 \quad q_c = \sigma'_r|_{r=a} \times (1 + \sqrt{3} \tan \phi) \quad (26)$$

371 where ϕ is assumed as the critical state friction angle. Thus the relationship between the
 372 normalised cone tip resistance Q , defined as $(q_c - p'_0)/p'_0$, and the in situ state parameter ξ_0
 373 is provided. The tests with Ticino sand (soil parameters can be found in Table 3) are conducted
 374 at an initial effective stress of $p'_0 = 74$ kPa (after a test of Ghafhazi and Shuttle 2008). The
 375 initial state parameter ξ_0 varies from -0.3 to 0.0, indicating an initial specific volume from 1.58
 376 to 1.88. The results are shown in Fig. 14, with a good comparison with data from the calibration

377 chamber tests (Shuttle and Jefferies 1998; Ghafghazi and Shuttle 2008). The calibration
378 chamber tests cover the initial mean stress in the range $50 \text{ kPa} < p'_0 < 500 \text{ kPa}$, and the initial
379 specific volume between 1.5 and 1.9. The results show that the normalised cone tip resistance
380 decreases with the value of initial state parameter, whereas the stress level was found to have
381 little effect on the $Q - \xi_0$ curve. It should be noted that, for application of the proposed solution,
382 further study is required for the back-analysis of CPT data. To estimate the properties of soils
383 based on the limited measured data, other techniques (e.g. probabilistic identification, Wang et
384 al. 2013; statistical characterization, Niazi et al. 2011) are desired to be incorporated into the
385 solution developed in this paper.

386

387 CONCLUSIONS

388 A new analytical solution for drained expansion of both spherical and cylindrical cavities with
389 a unified state parameter model for clay and sand (CASM) (Yu, 1998) is proposed in this paper.
390 CASM is a critical state soil model with two additional material constants, which has the ability
391 to capture the overall behaviour of either clay or sand under both drained and undrained loading
392 conditions. The developed cavity expansion solution with large strain analysis provides the
393 entire stress-strain histories of soils in the elastic and plastic regions. The approach of auxiliary
394 variable is employed for our drained analysis, which unifies the spherical/cylindrical scenarios
395 and clay/sand models.

396 As an illustration, both London clay and Ticino sand are modelled under various initial stress
397 conditions and initial state parameters. The parametric study investigates the effects on stress
398 paths and cavity expansion curves. Higher normalised cavity pressure (σ'_r/p'_0) is obtained for
399 the test with a higher overconsolidation ratio, which also results in a smaller elastic-plastic
400 radius. The increase of initial state parameter reduces the limiting cavity pressure but increases
401 the limiting specific volume on the critical state line. The results also show the ability of this
402 solution for modelling materials with different softening/hardening responses by modifying the
403 values of the stress-state coefficient and the spacing ratio. In addition, this analytical solution
404 provides a general analytical approach for drained cavity expansion problems using other
405 sophisticated critical state soil models. A simple application to the interpretation of CPT data
406 using the proposed solution shows a good comparison with data from the calibration chamber
407 tests. As shown by Yu (2000), it is expected that the new cavity expansion solution developed
408 in this paper can also be applied with success to other relevant geotechnical problems such as
409 pressuremeter tests, pile foundations and tunnelling in clay and sand under drained loading
410 condition.

411

412 ACKNOWLEDGMENTS

413 The authors would like to acknowledge financial support by “the Fundamental Research Funds
414 for the Central Universities” (No. 2017QNB10).

415

416 REFERENCES

417 Been, K. and Jefferies, M.G. 1985. A state parameter for sands. *Géotechnique*, 35(2): 99–112.

418 Cao, L.F., Teh, C.I. and Chang, M.F. 2001. Undrained cavity expansion in modified cam clay
419 I: Theoretical analysis. *Géotechnique*, 51(4): 323–334.

420 Carter, J.P., Booker, J.R. and Yeung, S.K. 1986. Cavity expansion in cohesive frictional soils.
421 *Géotechnique*, 36(3): 349–358.

422 Chen, S. L. and Abousleiman, Y.N. 2012. Exact undrained elasto-plastic solution for cylindrical
423 cavity expansion in modified cam clay soil. *Géotechnique*, 62(5): 447–456.

424 Chen, S.L. and Abousleiman, Y.N. 2013. Exact drained solution for cylindrical cavity
425 expansion in modified cam clay soil. *Géotechnique*, 63(6): 510–517.

426 Chen, S.L. and Abousleiman, Y.N. 2016. Drained and undrained analyses of cylindrical cavity
427 contractions by bounding surface plasticity. *Canadian Geotechnical Journal*, 53(9): 1398–
428 1411.

429 Chen, S.L. and Abousleiman, Y.N. 2017. Wellbore stability analysis using strain hardening
430 and/or softening plasticity models. *International Journal of Rock Mechanics & Mining
431 Sciences*, 93: 260–268.

432 Collins, I.F. and Stimpson, J.R. 1994. Similarity solutions for drained and undrained cavity
433 expansions in soils. *Géotechnique*, 44(1): 21–34.

434 Collins, I.F. and Yu, H.S. 1996. Undrained cavity expansions in critical state soils. *International
435 Journal for Numerical and Analytical Methods in Geomechanics*, 20(7): 489–516.

436 Collins, I.F., Pender, M.J. and Wang, Y. 1992. Cavity expansion in sands under drained loading
437 conditions. *International Journal for Numerical and Analytical Methods in Geomechanics*,
438 16(1): 3–23.

- 439 Jiang, M.J. and Sun, Y.G. 2012. Cavity expansion analyses of crushable granular materials with
440 state-dependent dilatancy. *International Journal for Numerical and Analytical Methods in*
441 *Geomechanics*, 36(6): 723–742.
- 442 Li, L, Li, J.P., Sun, D.A. and Gong, W.B. 2017. Unified Solution to Drained Expansion of a
443 Spherical Cavity in Clay and Sand. *International Journal of Geomechanics*, DOI:
444 10.1061/(ASCE)GM.1943-5622.0000909.
- 445 Mo, P.Q. and Yu, H.S. 2017. Undrained cavity expansion analysis with a unified state
446 parameter model for clay and sand. *Géotechnique*, 67(6): 503-515. DOI:
447 10.1680/jgeot.15.P.261.
- 448 Mo, P.Q., Marshall, A.M. and Yu, H.S. 2014. Elastic-plastic solutions for expanding cavities
449 embedded in two different cohesive-frictional materials. *International Journal for Numerical*
450 *and Analytical Methods in Geomechanics*, 38(9): 961–977.
- 451 Niaza, F.S., Mayne, P.W. and Wang, Y.H. 2011. Statistical Analysis of Cone Penetration Tests
452 and Soil Engineering Parameters at the National Geotechnical Experimentation Clay Site,
453 Texas A&M University, *Geo-Frontiers 2011*, 2998-3007.
- 454 Palmer, A.C. and Mitchell, R.J. 1971. Plane strain expansion of a cylindrical cavity in clay.
455 *Proceedings of the Roscoe Memorial Symposium*, Cambridge, UK: 588–599.
- 456 Rowe, P.W. 1962. The stress-dilatancy relation for static equilibrium of an assembly of
457 particles in contact. *Proc. Roy. Soc.*, 267: 500–527.
- 458 Russell, A.R. and Khalili, N. 2002. Drained cavity expansion in sands exhibiting particle
459 crushing. *International Journal for Numerical and Analytical Methods in Geomechanics*,
460 26(4): 323–340.
- 461 Schofield, A.N. and Wroth, C.P. 1968. *Critical state soil mechanics*. McGraw-Hill, New York,
462 NY, USA.
- 463 Sheng, D., Sloan, S.W. and Yu, H.S. 2000. Aspects of finite element implementation of critical
464 state models. *Comput. Mech.*, 26(2): 185-196.
- 465 Vesic, A.S. 1972. Expansion of cavities in infinite soil mass. *ASCE Journal of Soil Mechanics*
466 *and Foundations Division* 98(SM3), 5–290.
- 467 Vrakas, A. and Anagnostou, G. 2014. A finite strain closed-form solution for the elastoplastic
468 ground response curve in tunnelling. *International Journal for Numerical and Analytical*
469 *Methods in Geomechanics*, 38: 1131–1148.

- 470 Wang, Y., Huang, K. and Cao, Z.J. 2013. Probabilistic identification of underground soil
471 stratification using cone penetration tests. *Canadian Geotechnical Journal*, 50: 766-776.
- 472 Wroth, C.P. 1984. Interpretation of in situ soil tests. *Géotechnique*, 34(4): 449–489.
- 473 Wroth, C.P. and Bassett, N. 1965. A stress-strain relationship for the shearing behaviour of
474 sand. *Géotechnique*, 15(1): 32–56.
- 475 Yu, H.S. 1998. CASM: A unified state parameter model for clay and sand. *International Journal*
476 *for Numerical and Analytical Methods in Geomechanics*, 22(8): 621–653.
- 477 Yu, H.S. 2000. *Cavity Expansion Methods in Geomechanics*, Kluwer Academic Publishers,
478 Dordrecht, The Netherland.
- 479 Yu, H.S. 2006. *Plasticity and Geotechnics*, Springer, New York, NY, USA.
- 480 Yu, H.S. and Houlsby, G.T. 1991. Finite cavity expansion in dilatant soils: loading Analysis.
481 *Géotechnique*, 41(2): 173–183.

482

483

484 LIST OF FIGURES:

485 Fig. 1. Geometry and kinematics of cavity expansion.

486 Fig. 2. A general stress-state relation for both clay and sand in: (a) $\ln p' - v$ space; (b)
487 $p'/p'_y - q/(M \cdot p'_y)$ space.

488 Fig. 3. Comparisons between the proposed solution and results after solution of Chen and
489 Abousleiman (2013) for the Modified Cam-clay model.

490 Fig. 4. Stress paths for $a/a_0 = 1$ to 10 with variation of overconsolidation ratio σR_0 : (a)
491 spherical scenario; (b) cylindrical scenario.

492 Fig. 5. Cavity expansion curves for $a/a_0 = 1$ to 10 with variation of overconsolidation
493 ratio σR_0 : (a) spherical scenario; (b) cylindrical scenario.

494 Fig. 6. Variations of elastic-plastic radius c for $a/a_0 = 1$ to 10 with overconsolidation ratio
495 σR_0 : (a) spherical scenario; (b) cylindrical scenario.

496 Fig. 7. Effect of model constants n and r^* on stress paths for clay: (a) spherical scenario;
497 (b) cylindrical scenario.

498 Fig. 8. Effect of model constants n and r^* on cavity expansion curves for clay: (a) spherical
499 scenario; (b) cylindrical scenario.

500 Fig. 9. Cavity expansion curves for $a/a_0 = 1$ to 10 with variation of initial state parameter
501 ξ_0 : (a) spherical scenario; (b) cylindrical scenario.

502 Fig. 10. Stress paths in $\ln p' - v$ space for $a/a_0 = 1$ to 10 with variation of initial state
503 parameter ξ_0 : (a) spherical scenario; (b) cylindrical scenario.

504 Fig. 11. Stress paths in $\ln p' - v$ space for $a/a_0 = 1$ to 10 with variation of initial mean
505 stress p'_0 : (a) spherical scenario; (b) cylindrical scenario.

506 Fig. 12. Effect of model constants n and r^* on cavity expansion curves for sand: (a)
507 spherical scenario; (b) cylindrical scenario.

508 Fig. 13. Effect of model constants n and r^* on stress paths in $\ln p' - v$ space for sand: (a)
509 spherical scenario; (b) cylindrical scenario.

510 Fig. 14. Prediction of the relationship between normalised cone tip resistance and initial
511 state parameter.

512 LIST OF TABLES:

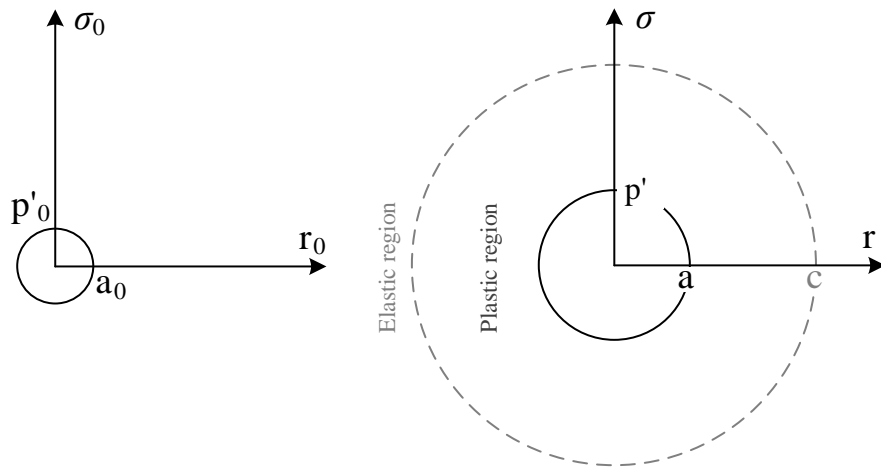
513 Table 1. Soil model parameters and initial conditions for validation of the proposed solution.

514 Table 2. Soil model parameters and initial conditions for London clay.

515 Table 3. Soil model parameters and initial conditions for Ticino sand under $p'_0 = 200 \text{ kPa}$.

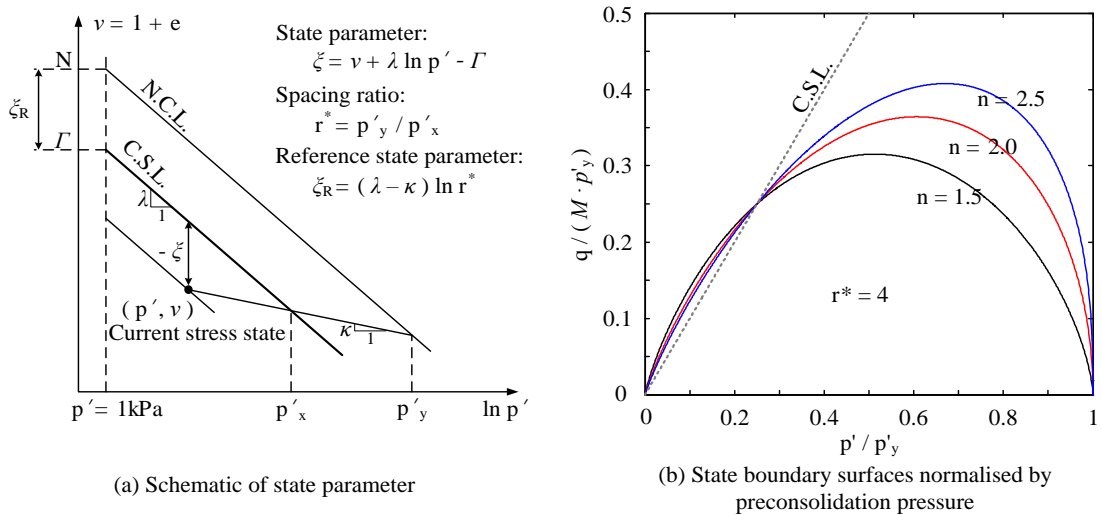
516 Table 4. Soil model parameters and initial conditions for Ticino sand under $p'_0 =$
517 $400, 600, 800 \text{ kPa}$.

518



520 (a) Initial cavity before expansion (b) Cavity after expansion

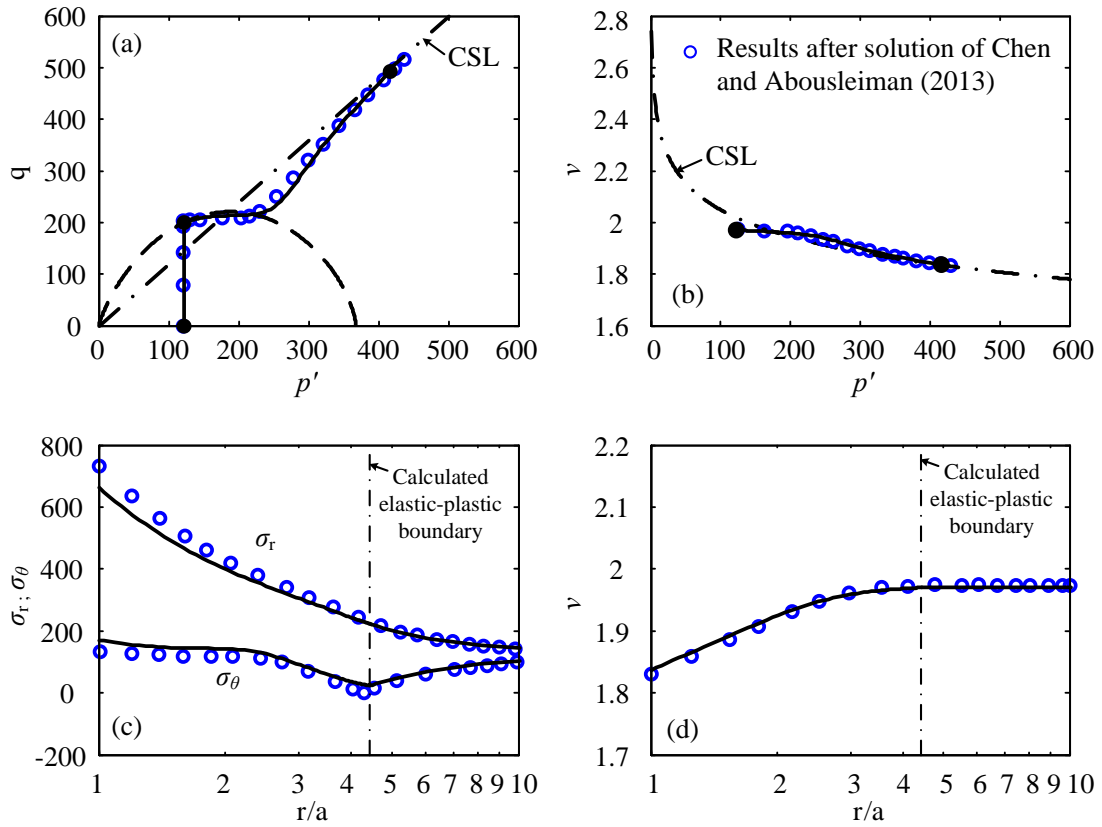
521 Fig. 1. Geometry and kinematics of cavity expansion.



522 (a) Schematic of state parameter (b) State boundary surfaces normalised by

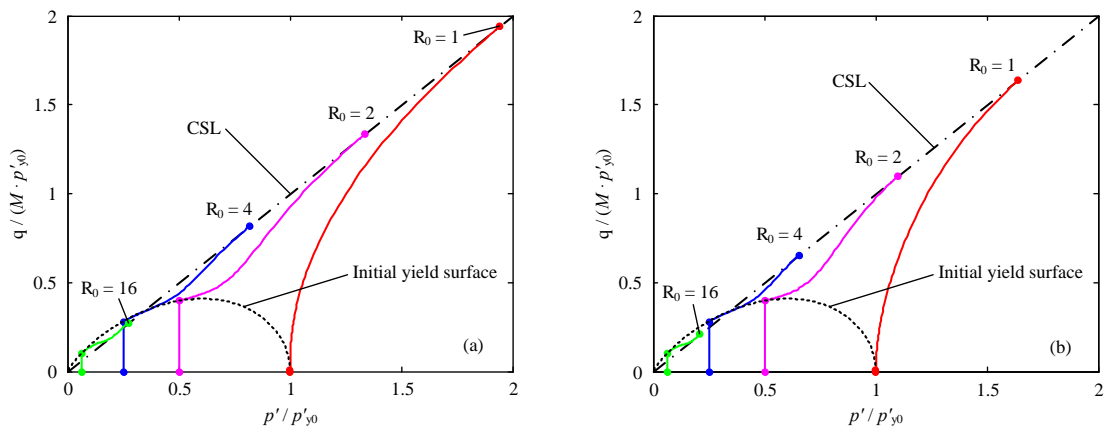
523 Fig. 2. A general stress-state relation for both clay and sand in: (a) $\ln p' - v$ space; (b)

524 $p' / p'_y - q / (M \cdot p'_y)$ space.



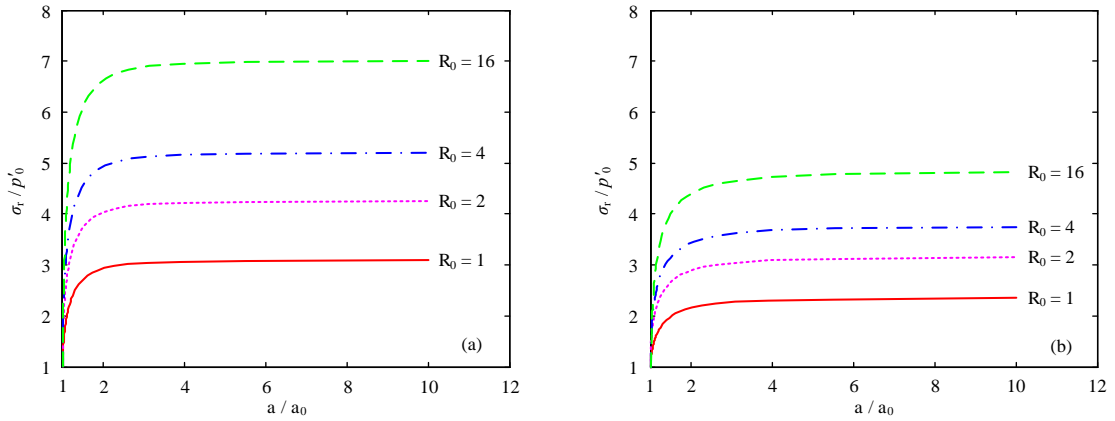
526

527 Fig. 3. Comparisons between the proposed solution and results after solution of Chen and
 528 Abousleiman (2013) for the Modified Cam-clay model.



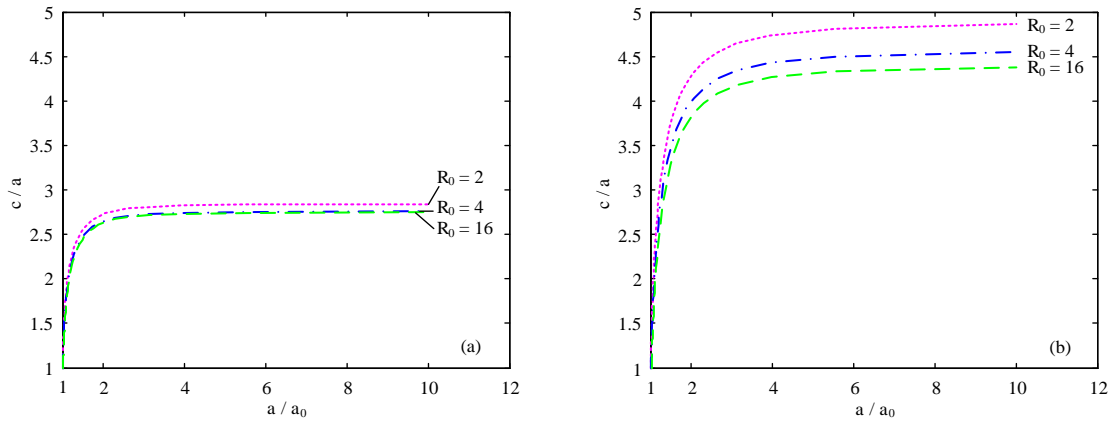
529

530 Fig. 4. Stress paths for $a/a_0 = 1$ to 10 with variation of overconsolidation ratio R_0 : (a)
 531 spherical scenario; (b) cylindrical scenario.



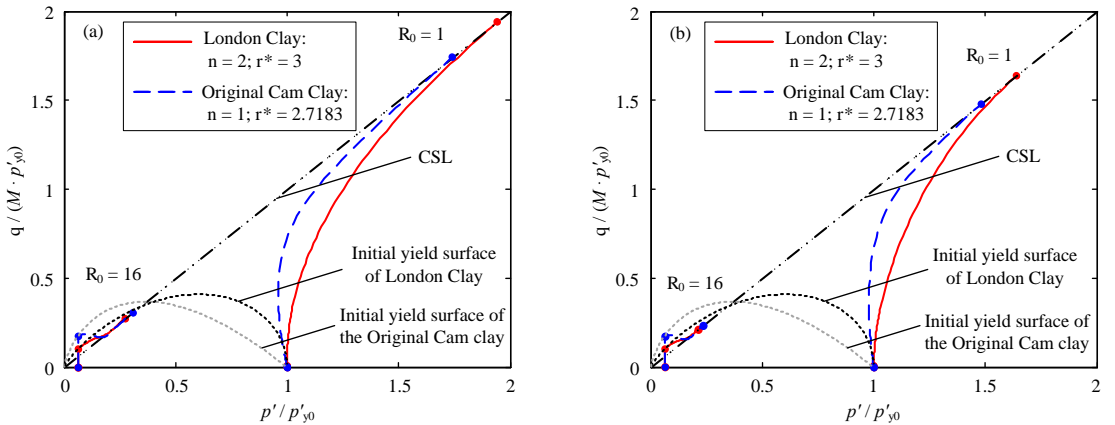
532

533 Fig. 5. Cavity expansion curves for $a/a_0 = 1$ to 10 with variation of overconsolidation ratio
 534 $\text{of } R_0$: (a) spherical scenario; (b) cylindrical scenario.



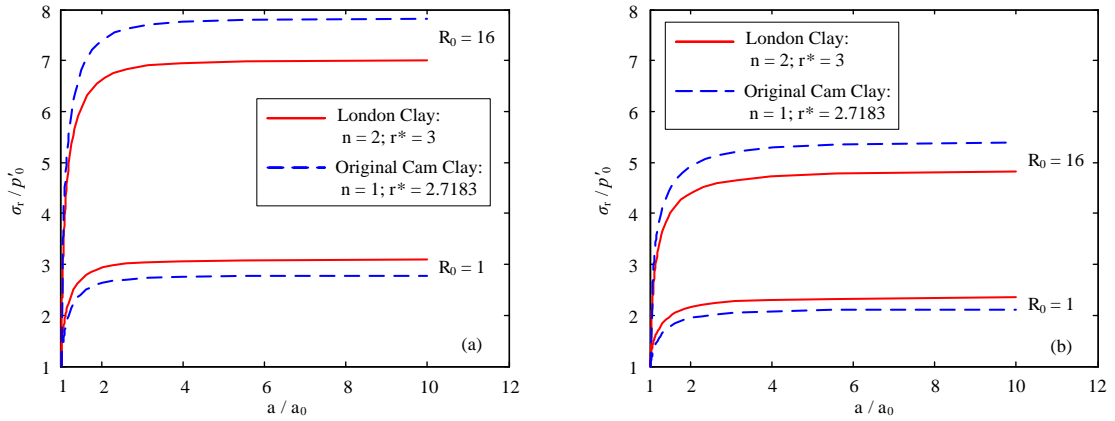
535

536 Fig. 6. Variations of elastic-plastic radius c for $a/a_0 = 1$ to 10 with overconsolidation ratio $\text{of } R_0$: (a) spherical scenario; (b) cylindrical scenario.



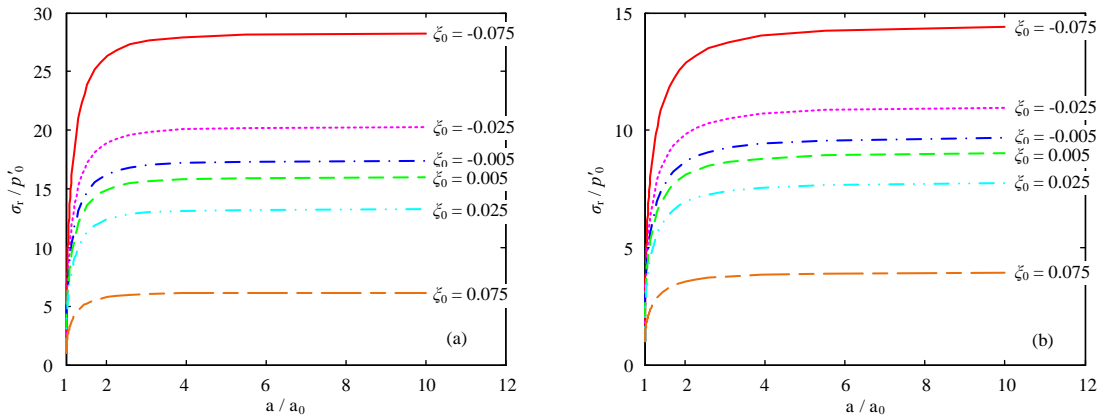
538

539 Fig. 7. Effect of model constants n and r^* on stress paths for clay: (a) spherical scenario; (b)
 540 cylindrical scenario.



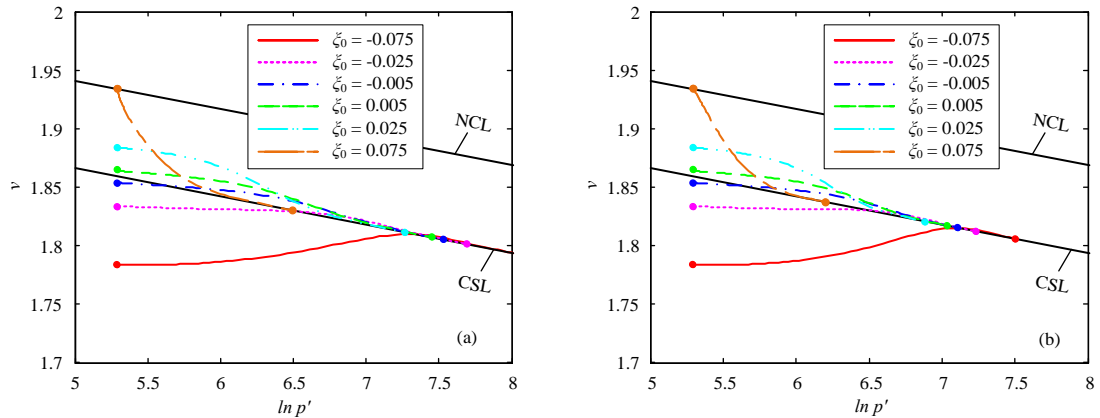
541

542 Fig. 8. Effect of model constants n and r^* on cavity expansion curves for clay: (a) spherical
543 scenario; (b) cylindrical scenario.



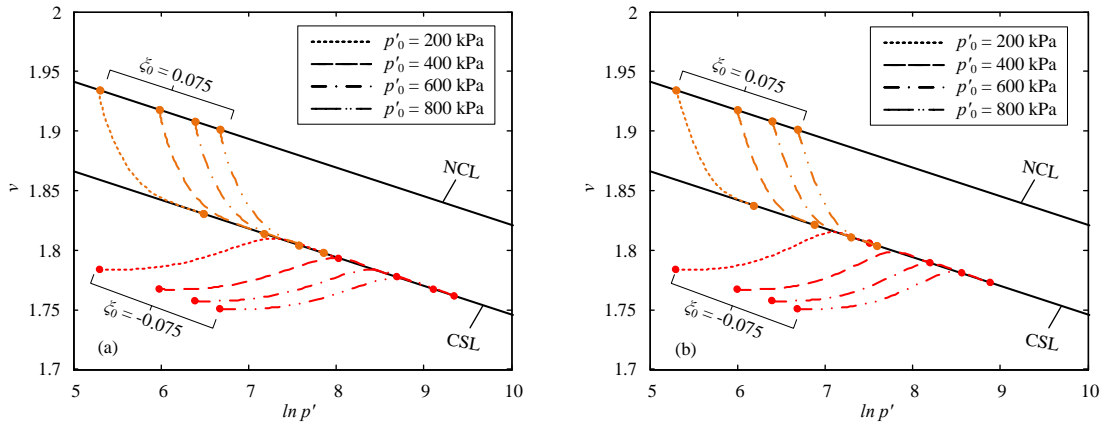
544

545 Fig. 9. Cavity expansion curves for $a/a_0 = 1$ to 10 with variation of initial state parameter
546 ξ_0 : (a) spherical scenario; (b) cylindrical scenario.



547

548 Fig. 10. Stress paths in $\ln p' - v$ space for $a/a_0 = 1$ to 10 with variation of initial state
549 parameter ξ_0 : (a) spherical scenario; (b) cylindrical scenario.



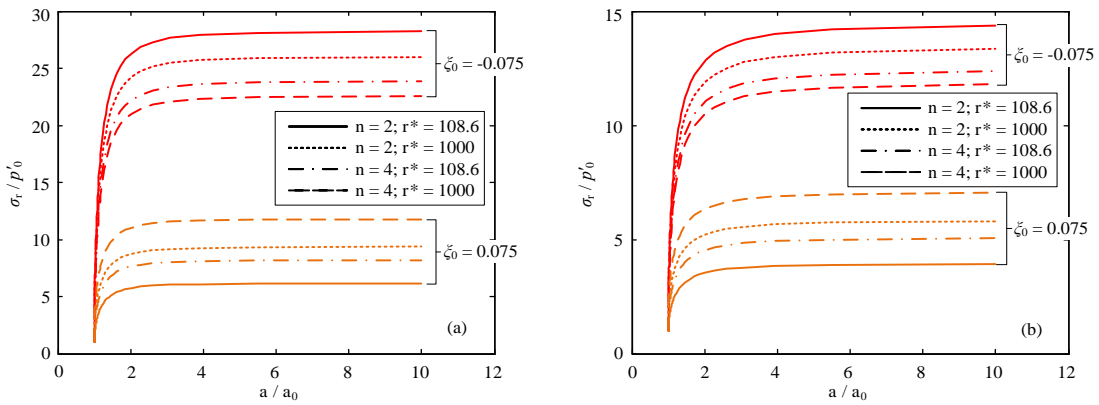
550

551

Fig. 11. Stress paths in $\ln p' - v$ space for $a/a_0 = 1$ to 10 with variation of initial mean

552

stress p'_0 : (a) spherical scenario; (b) cylindrical scenario.



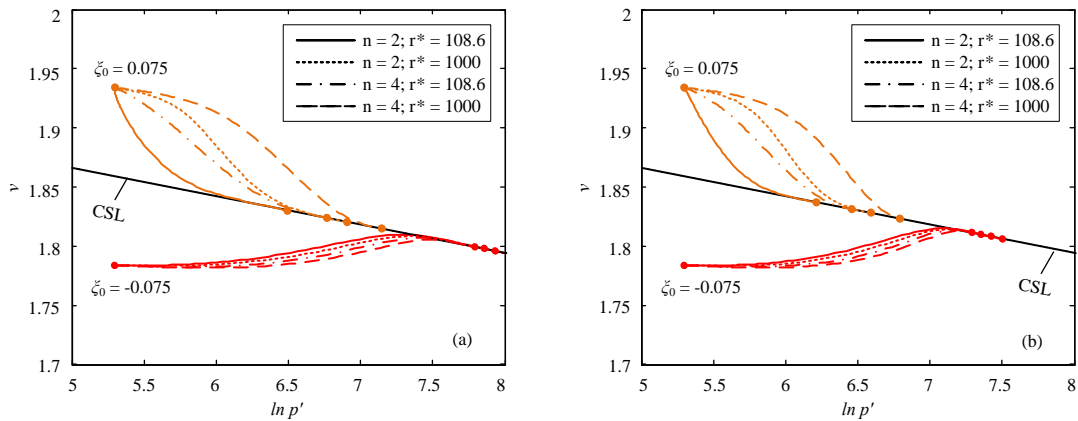
553

554

Fig. 12. Effect of model constants n and r^* on cavity expansion curves for sand: (a) spherical

555

scenario; (b) cylindrical scenario.



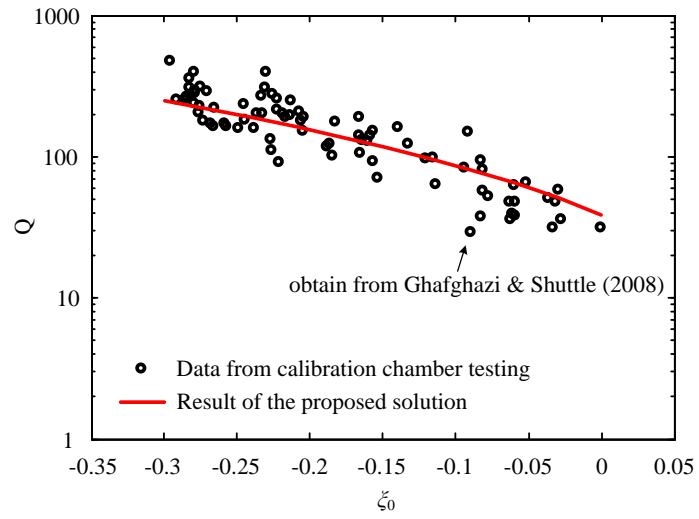
556

557

Fig. 13. Effect of model constants n and r^* on stress paths in $\ln p' - v$ space for sand: (a)

558

spherical scenario; (b) cylindrical scenario.



559

560 Fig. 14. Prediction of the relationship between normalised cone tip resistance and initial
 561 state parameter.

562

563

564 TABLES:

565 Table 1. Soil model parameters and initial conditions for validation of the proposed solution.

$$\Gamma = 2.74; \lambda = 0.15; \kappa = 0.03; \mu = 0.278; M = 1.2; R_0 = 3; \nu_0 = 1.97$$

	This study	Chen and Abousleiman (2013)
Spacing ratio r^*	2.0	-
Stress-state coefficient n	1.5	-
Initial stress p'_0 (kPa)	122.6	120
G_0 (kPa)	3575	4113

566

567 Table 2. Soil model parameters and initial conditions for London clay.

$$\Gamma = 2.759; \lambda = 0.161; \kappa = 0.062; \mu = 0.3; n = 2.0; r^* = 3.0$$

$$\phi_{tx} = 22.75^\circ: M = 0.8879 \text{ (spherical)}, M = 0.8640 \text{ (cylindrical)}$$

Overconsolidation ratio R_0	1	2	4	6	
Initial specific volume ν_0	2.0	2.0	2.0	2.0	
Initial stress p'_0 (kPa)	219.15	143.11	93.45	39.84	
Initial state parameter ξ_0	0.1088	0.0401	-0.0285	-0.1657	
G_0 (kPa)	spherical	3263	2131	1391	593
	cylindrical	2828	1847	1206	514

568

569 Table 3. Soil model parameters and initial conditions for Ticino sand under $p'_0 = 200 \text{ kPa}$.

$$\Gamma = 1.986; \lambda = 0.024; \kappa = 0.008; \mu = 0.3; n = 2.0; r^* = 108.6$$

$$\phi_{tx} = 32.0^\circ: M = 1.2872 \text{ (spherical)}, M = 1.1756 \text{ (cylindrical)}$$

Initial state parameter ξ_0	-0.075	-0.025	-0.005	0.005	0.025	0.075	
Initial stress p'_0 (kPa)	200	200	200	200	200	200	
Overconsolidation ratio R_0	11792	518.1	148.4	79.5	22.8	1.0	
Initial specific volume ν_0	1.7838	1.8338	1.8538	1.8638	1.8838	1.9338	
G_0 (kPa)	spherical	20583	21160	21390	21506	21737	22314
	cylindrical	17838	18338	18538	18638	18838	19338

570

571 Table 4. Soil model parameters and initial conditions for Ticino sand under $p'_0 =$
 572 400, 600, 800 kPa.

Initial state parameter ξ_0		-0.075 ($R_0 = 11792$)			0.075 ($R_0 = 1$)		
Initial stress p'_0 (kPa)		400	600	800	400	600	800
Initial specific volume v_0		1.7672	1.7575	1.7506	1.9172	1.9075	1.9006
G_0 (kPa)	spherical	40782	60836	80796	44243	66028	87719
	cylindrical	35344	52724	70023	38344	57224	76023

573

574